

Magnetic turbulence in cool cores of galaxy clusters

Torsten A. Enßlin¹ and Corina Vogt^{1,2}

¹ Max-Planck-Institut für Astrophysik, Karl-Schwarzschild-Str.1, Postfach 1317, 85741 Garching, Germany

² ASTRON, P.O.Box 2, 7990 AA Dwingeloo, The Netherlands

December 24, 2018

Abstract. We argue that the recently reported Kolmogorov-like magnetic turbulence spectrum in the cool core of the Hydra A galaxy cluster can be understood by kinetic energy injection by active galaxies which drive a turbulent non-helical magnetic dynamo into its saturated state. Although dramatic differences exist between small-scale dynamo scenarios, their saturated state is expected to be quite similar, as we show for three scenarios: the *flux rope dynamo*, the *fluctuation dynamo*, and the *explosive dynamo*. Based on those scenarios, we develop an analytical model of the hydrodynamical and magnetic turbulence in cool cores. The model implies magnetic field strengths which fit well to Faraday rotation measurements and minimum energy estimates for the sample of cool core clusters having such data available. Moreover, predictions for magnetic fields in clusters for which the appropriate observational information is still missing, and for yet unobserved quantities like the hydrodynamical turbulence velocity and characteristic length-scale are provided. The underlying dynamo models suggest some level of magnetic intermittency and possibly a large-scale hydrodynamic viscosity. We concluded that the success of the model to explain the field strength in cool core clusters indicates that in general cluster magnetic fields are directly reflecting hydrodynamical turbulence, also in clusters without cool cores.

Key words. Galaxies: cluster: general – cooling flows – Magnetic Fields – Turbulence – X-rays: galaxies: clusters – intergalactic medium

1. Introduction

1.1. Magnetic fields in cool cores

Galaxy clusters contain magnetised plasma on cluster scales, as radio-synchrotron emission of relativistic electrons reveals in form of the so-called *cluster radio halos*. The origin, the strength and geometry of these magnetic fields is still a mystery.

With the emerging of the first theories of magnetic dynamos (Batchelor 1950; Kazantsev 1967; Zeldovich et al. 1990), it was proposed that the cluster magnetic fields are the product of turbulence acting on a seed magnetic field. The seed field could be a remnant of non-equilibrium processes in the early Universe, or due to some weak magnetisation caused by galactic outflows in form of winds and radio plasma (for a review see Widrow 2002).

Initially, wakes of the weakly sonic galaxy motions were thought to be the main driver of the intra-cluster turbulence¹. However, it was realised using numerical simulations of large-scale structure formation that the violent mergers of galaxy clusters are a much more powerful source of turbulence (e.g. Tribble 1993). In numerical simulations of magnetic field amplification, the merger driven turbulence of galaxy clusters

seems to be well capable to reproduce the typical field values of clusters².

It is therefore a bit surprising that the strongest magnetic fields seem to be located in the centres of clusters which were dynamically the most relaxed, since the last major merger was long ago. These *cooling flow* (now *cool core*) clusters had time to develop a cool, dense central region due to the cooling instability of optically thin X-ray emission of cooling gas. The magnetic fields reported for those cooling flow regions inferred by Faraday rotation studies were extraordinary strong (up to $50 \mu\text{G}$) compared to the few μG fields reported for non-cooling flow clusters (for recent reviews see Carilli & Taylor 2002; Govoni & Feretti 2004). It was speculated, that the strong fields could be a result of the compressional flow in the cooling flow (Soker & Sarazin 1990).

However, Chandra and XMM observations revealed that the standard cooling flow picture, in which unheated gas cools down to neutral gas temperatures, must be incorrect, since the expected amount of line emission of cold ($< 0.3 \text{ keV}$) gas or the expected number of stars formed from the condensing gas was not detected³. Therefore a heat source has to be present which balances the cooling of the coldest gas. Since the theo-

¹ e.g. Jaffe (1980); Roland (1981); Ruzmaikin et al. (1989); Goldman & Rephaeli (1991); De Young (1992)

² Dolag et al. (1999); Roettiger et al. (1999b); Dolag et al. (2002)

³ Heckman et al. (1989); Fabian et al. (1991); Hansen et al. (1995); Allen (1995); Jaffe & Bremer (1997); Smith et al. (1997); O'Dea et al. (1998); Crawford et al. (1999); Donahue et al. (2000); Edge (2001);

retical scenario associated with the term *cooling flow* has been ruled out recently, the solely observationally motivated term *cool core* is used in the following.

The energy losses of the cool core have to be balanced by a similar energy injection. There were two main proposals⁴ for the heat source in cool cores:

- (i) Thermal conductivity, which is close to Spitzer's estimate, and therefore not suppressed by magnetic fields. This would allow the inward transport of heat from the hotter environmental intra-cluster medium (ICM)⁵.
- (ii) Dissipation of mechanical energy released by the expansion and buoyant motion of radio bubbles inflated by the radio galaxies which are typically found in the centre of a cool core of a galaxy cluster⁶.

The thermal conduction scenario (i) as the only heat injection mechanism into cool cores faces severe problems in terms of fine-tuning the required energy injection, and explaining the existence of cold gas clouds which need sufficient insulation from the keV gas (Soker 2003; Nipoti & Binney 2004). Too strong conduction would erase the cool core, but too weak conduction can not prevent the cooling catastrophe. Therefore a conductively heated cool core should be unstable.

The scenario (ii) in which the central radio galaxy balances the radiative energy losses of the cool core provides naturally fine tuning in form of a self-adapting feedback mechanism: If the radio galaxy activity is triggered by cold gas condensing out of the cool core onto the central galaxy, the galaxy activity increases until it disrupts further accretion (Churazov et al. 2001).

In this work we assume scenario (ii), not only since it is – at least in our view – theoretically more compelling, but also because it predicts a certain level of hydrodynamical turbulence, which can be compared to the level required to explain the cool core magnetic fields by magnetic dynamo theory.

There have been some reports on observed signatures of turbulent flows in cool cores of galaxy clusters, and the scenario (ii) investigated here seems to become widely accepted, at least as a working hypothesis (e.g. Loewenstein & Fabian 1990; Churazov et al. 2001; Böhringer et al. 2002; Churazov et al. 2002, 2004).

Oegerle et al. (2001); Salomé & Combes (2003); Edge & Frayer (2003)

⁴ There are also other mechanisms discussed in the literature, e.g. the influence of a cosmic ray population (Chandran 2004; Cen 2005).

⁵ Malyshkin (2001); Narayan & Medvedev (2001); Voigt et al. (2002); Ruszkowski & Begelman (2002); Cho et al. (2003); Soker et al. (2004); Voigt & Fabian (2004); Soker (2004); Jubelgas et al. (2004); Chandran & Maron (2004); Dolag et al. (2004)

⁶ Churazov et al. (2001); Brüggen & Kaiser (2001); Quilis et al. (2001); Brüggen et al. (2002); Chandran (2004); Hoeft & Brüggen (2004); Dennis & Chandran (2005). There have been also observations of hot gas bubbles (Mazzotta et al. 2004), which may also contribute to the cool core heating in a very similar way as the radio bubbles (Soker & Pizzolato 2005)

1.2. Observations of cluster magnetic fields

Magnetic fields in normal clusters and cool core clusters have revealed their existence by the diffuse radio halo emission in many clusters and radio mini-halos in cool core regions. Furthermore, the Faraday rotation of linearly polarised radio emission traversing the intra-cluster medium proves independently the existence of intra-cluster magnetic fields. If the Faraday active medium is external to the source of the polarised emission, one expects the change in polarisation angle to be proportional to the squared wavelength. The proportionality factor is called the rotation measure (*RM*). This quantity can be evaluated in terms of the line of sight integral over the product of the electron density and the magnetic field component along the line of sight.

Magnetic fields in non-cool core clusters of galaxies detected through Faraday rotation measurements are of the order of a few μG . Kim et al. (1991) measured field strengths of about 2 μG on scales of 10 kpc in a statistical sample of point sources observed through the Coma cluster. Clarke et al. (2001), Clarke (2004), and Johnston-Hollitt & Ekers (2004) derive similar field strengths of several μG in various samples of point sources observed within and through various low redshift clusters in the northern and southern hemisphere. The analysis of *RM* maps of extended radio sources have lead to the same conclusion (e.g. Feretti et al. 1995, 1999; Taylor et al. 2001; Govoni et al. 2001; Eilek & Owen 2002; Vogt & Enßlin 2003).

However, the analysis of Faraday rotation measurements of extended radio sources in the centre of cool core clusters reveal higher magnetic field strengths. Such an analysis has been done for the Centaurus cluster by Taylor et al. (2002), for A1958 (better known as 3C295) by Perley & Taylor (1991), for A1795 by Ge & Owen (1993), for Cygnus A by Dreher et al. (1987) and for Hydra A by Taylor & Perley (1993). From these *RM* measurements, magnetic field strengths of 10 to 40 μG have been reported for the cores of these cool core clusters on scales of 3–5 kpc.

These rather large field values for cool core clusters have been revised in the case of Hydra A by a recent analysis of the observational data. A high quality Faraday rotation map of the north lobe of Hydra A produced by the novel PACERMAN algorithm (Dolag et al. 2005; Vogt et al. 2005) based on the data of Taylor & Perley (1993) was analysed by Vogt & Enßlin (2005). They used a maximum likelihood estimator for the derivation of the magnetic power spectra, based on the theory of turbulent Faraday screens (Enßlin & Vogt 2003; Vogt & Enßlin 2003), and also using the most up-to date gas density profile of the cool core, which turned out to make a crucial difference. Thereby, a magnetic field strength of $7 \pm 2 \mu\text{G}$ was found in the centre of the cool core region of the Hydra A cluster, which is still a significantly larger field than reported for non-cool core clusters. Vogt & Enßlin (2005) measured the detailed magnetic power spectrum from the Hydra A dataset, which revealed a Kolmogorov-type spectrum on small scales indicating turbulence (see Fig. 1).

It has been debated, if the magnetic fields seen by the Faraday effect exist on cluster scales in the ICM, or in a mix-

ing layer around the radio plasma which emits the polarised emission (Bicknell et al. 1990; Rudnick & Blundell 2003). However, there is no valid indication of a source local Faraday effect in the discussed cases (Enßlin et al. 2003), and the Faraday rotation signal excess of radio sources behind clusters compared to a field control sample strongly supports the existence of strong magnetic fields in the wider ICM (Clarke et al. 2001; Johnston-Hollitt & Ekers 2004; Clarke 2004).

The morphological structure of magnetic fields in galaxy cluster is difficult to obtain due to the projection effects in radio observations. However, there are situations in which the magnetic fields are illuminated in only sheet like sub-volumes of clusters. This happens whenever short-lived ultra-relativistic electrons are injected at a shock wave travelling through the ICM. The electrons usually lose their energy before the shock wave could travel far away. Thereby the electrons produce synchrotron radio emission from a nearly sheet-like volume. This emission forms likely the so called giant radio relics (Enßlin et al. 1998a; Roettiger et al. 1999a). High resolution radio polarisation maps of the relic in Abell 2256, which is one of the largest radio relics known, reveal that the magnetic fields are organised in filaments or sheets with an aspect ratio of at least 5 (Clarke & Enßlin 2005). Furthermore, the Faraday rotation map of 3C465 reveals stripy patterns (Eilek & Owen 2002), also suggesting the existence of intermittent fields in galaxy clusters. The presence of thermally isolated elongated cool H- α filaments in the core of the Centaurus cluster is also best understood by the existence of filamentary magnetic fields in that environment (Crawford et al. 2005).

1.3. Structure of the paper

The paper is structured as follows: In Sect. 2 we introduce the turbulent dynamo and summarise its expected and observed signatures in galaxy clusters, mainly based on the above mentioned estimate of the magnetic power-spectrum in the Hydra A cluster core. In Sect. 3 we develop a steady-state analytical description of the expected magnetic turbulence due to the stirring motion of buoyant radio bubbles from the central galaxy, which is assumed to regulate the energy content of the cool core. This is applied in Sect. 4 to a number of prominent cool core clusters, and compared to existing information on magnetic fields whenever available. Sect. 5 contains our conclusions.

Throughout the paper, we assume a Hubble constant of $H_0 = 70 \text{ km/s/Mpc}$, and translate literature values of luminosities, length scales, electron densities and magnetic field strengths derived from Faraday rotation measurements to this value without further notice.

2. Turbulent magnetic dynamo

2.1. Dynamo concepts

The Kolmogorov-like magnetic power spectrum in the cool core of the Hydra A cluster indicates that the magnetic fields are shaped and probably amplified by hydrodynamical turbulence (e.g. De Young 1992). Therefore, it seems most promising to seek the origin of the observed magnetic power spec-

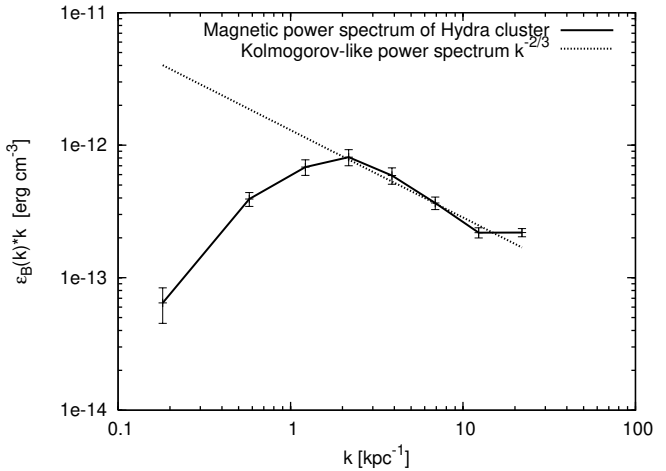


Fig. 1. Magnetic turbulence in the centre of the cool core cluster Hydra A as derived from the Faraday rotation map of the northern radio lobe of Hydra A by Vogt & Enßlin (2005). An angle of 45° was assumed in this figure between the line of sight and the approaching north-lobe. Variation of this angle changes the overall normalisation of the spectrum, but not its shape. The right-most data point is likely to be contaminated by observational noise in the Faraday map. A central root-mean-square magnetic field strength of $B_{\text{rms}} = 7.3 \pm 0.2 \pm 2 \mu\text{G}$ and a magnetic autocorrelation length of $\lambda_B = 2.8 \pm 0.2 \pm 0.5 \text{ kpc}$ was derived by Vogt & Enßlin (2005). The first errors are the statistical uncertainties due to the limited statistics, whereas the systematic error is reflecting the uncertainties in the geometry of the radio source and the Faraday screen.

trum in the theories of turbulent dynamos. Note, that a very similar view and approach are used in the recent work by Subramanian et al. (2006), in which the magnetic fields in non-cooling core clusters were also assumed to be maintained by turbulence. In that environment the turbulence is due to merger events and galaxy motions, whereas here it is due to the inflation and buoyant motion of radio bubbles.

Since cool cores of galaxy clusters are not believed to rotate, the gas flow is probably non-helical and the galactic dynamo theories do not apply here. Instead, the non-helical turbulent dynamo (also called small-scale dynamo) should operate if the gas flow is sufficiently random, as it would be in the case of developed turbulence.

The physical details of the small-scale dynamo are still debated. However, as it turns out, the exact nature of the small scale dynamo is of minor importance for an understanding of cool core magnetic fields. The observed magnetic field is probably determined by the saturated state of such a dynamo, provided the dynamo had sufficient time to amplify seed fields to the dynamically relevant strength. This condition is fulfilled if either the dynamo is very efficient, permitting the very weak primordial fields to be amplified, or if the dynamo can start on an existing, relatively strong magnetisation, which is only a few orders of magnitude below the saturation level. There are arguments in favour of both pre-conditions being fulfilled, which we discuss briefly.

The random gas motion would stretch and fold any initial seed magnetic fields and lead to an exponential growth of the magnetic energy density with time with the characteristic time-scale being the eddy-turnover time. This proceeds as long as the dynamical back-reaction of the magnetic field is unimportant. The folding operations of the flow form small-scale magnetic reversals perpendicular to the local field directions (Schekochihin et al. 2002). Magnetic diffusivity limits the scales to be of the order of $\lambda_B \sim \lambda_T R_m^{-1/2}$, where λ_T is the turbulence injection scale, and R_m is the magnetic Reynolds-number (Ruzmaikin et al. 1989). The typical bending radius of the fields should be of the order of the turbulence length-scale λ_T .

This picture has been criticised by Goldshmidt & Rephaeli (1993) for being unable to explain cluster magnetic fields. Their main objective is that the transverse size of the magnetic structures λ_B should be extremely small, since the magnetic Reynolds number is typically $R_m \sim 10^{28..29}$ in a cluster environment, leading in λ_B of the order of a light second. However, magnetic structures with kpc size are required to accommodate the observed Faraday rotation values with physically plausible cluster magnetic fields. This reasoning have lead Goldshmidt & Rephaeli (1993) to argue for a galactic origin of the intra cluster magnetic fields. And indeed, rough estimates of the magnetisation of the intra cluster medium indicate that galactic outflows in magnetised winds and relativistic plasma jets should lead to a substantial seed magnetisation⁷.

The small scale dynamo picture can only be reconciled with the observations if the huge magnetic Reynolds number gets replaced by a much lower effective value. It was pointed out by Subramanian (1999) that the gas motions induced by the magnetic forces lead to a diminishing of the magnetic field strength, which can be expressed approximately as an effective magnetic diffusivity. This diffusivity increases with growing magnetic field strength, leading to a decreasing effective magnetic Reynolds number permitting the magnetic structures to grow to larger spatial scales. On larger scales more turbulent energy density is available in a Kolmogorov cascade, thus larger field strengths can be accommodated. Larger field strengths imply a further decreased effective magnetic Reynolds number and therefore a further growth of the fields in strength and length scale. This process continues until a saturated state is reached. The magnetic *e*-folding time is of the order of the turbulent eddy time scale and might be sufficient to amplify even primordial magnetic fields in a cluster environment to their observed strength.

It was argued by Schekochihin et al. (2005) that plasma instabilities should lead to an accelerated regime of magnetic amplifications during the pre-saturation phase. Assuming an effective description for the plasma particle pitch angle scattering by the plasma-waves generated in the instabilities Schekochihin et al. (2005) showed that a nearly explosive production of magnetic fields from very weak primordial seed

⁷ Rees (1987), Daly & Loeb (1990), Chakrabarti et al. (1994), Enßlin et al. (1997, 1998b), Kronberg et al. (1999), Völk & Atoyan (2000), Kronberg et al. (2001), Bertone et al. (2005)

fields on cosmological negligible times-scales might be possible.

To summarise, although the details of the generation of dynamically relevant magnetic fields in galaxy clusters are still unclear, it seems that there are sufficient sources of magnetisation, and sufficiently efficient dynamo mechanisms present to amplify such fields in cosmological short times. The question for the interpretation of the observational data is in which state do we expect the fields to be at present. This requires an examination of the saturated dynamo state.

2.2. Saturated dynamo state

We start our investigation of the saturated state with the picture introduced by Subramanian (1999). As soon as the Lorentz-force becomes sufficiently strong, the fields do not follow the flow passively, but start to try to disentangle themselves. This back-reaction motion leads to an increase in the effective magnetic diffusivity, and therefore to a lower, renormalised magnetic Reynolds-number implying fields to become organised on larger scales. The Reynolds-number decreases until it reaches a critical value $R_c \sim 10 - 100$, below which the turbulent dynamo would stop to operate. The system reaches a saturated state, in which the magnetic correlation length scale

$$\lambda_B \sim \lambda_T R_c^{-1/2} \quad (1)$$

is solely determined by the turbulence length scale and the critical Reynolds number.

Schekochihin & Cowley (2006) acknowledge that their explosive dynamo alone fails to explain the observed level of cluster magnetisation, but only by up to one order of magnitude. Therefore, the remaining amplification and the saturated state should result from a conventional non-helical dynamo (e.g. Subramanian 1999). However, Schekochihin & Cowley (2006) speculate that the physics of the plasma instability driven dynamo still imprints on the saturated state, leading to a characteristic field strength with $\lambda_B \sim \lambda_T (v_{th,i}/v_T)^{1/2} (\rho_i/\lambda_T)^{1/8}$. Here, v_{th} and v_T are the ion and the turbulent velocity, respectively. ρ_i is the gyroradius of an ion within a magnetic field which is in equipartition with the turbulent energy density. We note, that this picture of the saturated state can be mathematically mapped onto the other picture by Subramanian (1999) if we define an effective magnetic Reynolds number of

$$R_c^* \sim \frac{v_T}{v_{th,i}} \left(\frac{\lambda_T}{\rho_i} \right)^{\frac{1}{4}} \quad (2)$$

which takes values in the range $10^{2..3}$ for cluster environments.

In the picture initially developed by Batchelor (1950); Kazantsev (1967); Zeldovich et al. (1990), the magnetic fields are highly intermittent: only a small fraction f_B of the volume is actually strongly magnetised, whereas the remaining volume $1 - f_B$ does not carry dynamically important magnetic fields. Zeldovich et al. (1990) and others (Ruzmaikin et al. 1989; Sokolov et al. 1990; Subramanian 1999) assumed the magnetised regions to be organised as magnetic flux ropes of volume $\lambda_T \lambda_B^2$ per eddy volume λ_T^3 . The occupied volume

fraction would be $f_B \sim \lambda_B^2/\lambda_T^2 \sim R_c^{-1}$. Such highly filamentary structures were not confirmed by numerical simulations. By using a spectral MHD code, Cho & Vishniac (2000) find for example that the magnetic autocorrelation functions exhibit only a moderate anisotropy on scales where the magnetic energy density peaks. However, numerical simulations in physical space indicate that the magnetic structures are more sheet-like with thickness λ_B (Brandenburg & Subramanian 2004; Schekochihin & Cowley 2006), leading to a $f_B \sim \lambda_B/\lambda_T \sim R_c^{-1/2}$ as assumed in Subramanian et al. (2006). Furthermore, as we explained in Sect. 1.2, radio observations of the cluster radio relic in Abell 2256 also strongly support the assumption of intermittent magnetic fields, probably of sheet like structure.

In order to allow for any geometry of the magnetic structures in the saturated state, we assume that they are effectively d -dimensional, giving

$$f_B \sim \frac{\lambda_T^d \lambda_B^{3-d}}{\lambda_T^3} \sim R_c^{-\frac{3-d}{2}}, \text{ with } 1 \leq d \leq 3. \quad (3)$$

Under the steady-state conditions of the saturated dynamo, the hydrodynamical dissipation of turbulent energy on scale λ_T and the relaxation of magnetic structures bent on the same scales λ_T should have the same time scales:

$$\tau_B \sim \frac{\lambda_T}{v_A^{\text{struct}}} = \lambda_T \sqrt{\frac{\rho}{2 \varepsilon_B^{\text{struct}}}} \quad (4)$$

$$\tau_T \sim \frac{\lambda_T}{v_T} = \lambda_T \sqrt{\frac{\rho}{2 \varepsilon_T}}, \quad (5)$$

where v_A^{struct} and $\varepsilon_B^{\text{struct}}$ are the Alfvénic velocity and energy density within the magnetic structures, and v_T and ε_T the turbulent velocity and energy density, respectively. Then $\tau_B \sim \tau_T$ implies that the magnetic fields within the structures are in equipartition with the environmental turbulent energy density, and the volume averaged magnetic energy density is therefore lower than these by the magnetic volume filling factor:

$$\varepsilon_B \sim \varepsilon_B^{\text{struct}} f_B \sim \varepsilon_T f_B \sim \varepsilon_T R_c^{-\frac{3-d}{2}}. \quad (6)$$

Thus, with the knowledge or assumption of the critical Reynolds-number R_c , and the effective dimensionality d of the magnetised regions it is possible to translate properties of the hydrodynamical turbulence to the magnetic turbulence and vice versa, under the assumption that the system is in the saturated dynamo state.

In the numerical examples, we will investigate three scenarios, which differ in assumed magnetic topology and critical magnetic Reynolds number:

1. Magnetic fields mostly organise in flux tubes ($d = 1$, $R_c = 20, \Rightarrow f_B = 0.05$). This scenario reflects the original assumption on turbulent magnetic structures by Zeldovich et al. (1990) but modified with the concept of the renormalised Reynolds number (Subramanian 1999). Here we consider it to investigate the induced hydrodynamical viscosity on large scales, since there are published predictions for this quantity in the flux rope scenario (Longcope et al. 2003).
2. Magnetic fields mostly organise in sheets and ribbons ($d = 2$, $R_c = 35, \Rightarrow f_B = 0.17$). This scenario is more in agreement with recent numerical simulations, as argued by Subramanian et al. (2006).⁸
3. The assumed saturated state of the explosive dynamo of Schekochihin & Cowley (2006), which we characterise by $d = 2$ dimensions and by an effective Reynolds number $R_c = R_c^*$ provided by Eq. 2.

The scaling of any quantity with the parameters R_c and d will also be provided, so that this theory may stay applicable even in case the adopted values need readjustments.

2.3. Magnetic viscosity

In the saturated dynamo state, the magnetic fields are not passively following the hydrodynamical flow of the bulk motion, but possess an independent velocity component due to the Lorentz force. This should lead to a slippage of strongly and weakly magnetised regions relative to each other, possibly causing some friction due to induction of small scale eddies in the wakes of the magnetic structures. For the flux rope dynamo scenario, Longcope et al. (2003) give the expected viscosity on large spatial scales in the saturated state to be of the order of 4% of the turbulent diffusivity $\kappa_T \approx v_T \lambda_T/3$, thus

$$\kappa_{\text{visc}} \approx 0.04 \frac{v_T \lambda_T}{3}. \quad (7)$$

Also in the scenario of mainly 2-dimensional magnetic structures, one would expect such viscous effects, but no estimates of the viscosity exist to our knowledge.

2.4. Signatures

According to the scenario described above, the magnetic fields in the turbulent cool cores of galaxy clusters should exhibit the following properties:

- A. The magnetic power spectrum should either reflect the hydrodynamical power spectrum due to their dynamical coupling, just with a lower normalisation and on smaller spatial scales or the small-scale magnetic fluctuations are expected to follow a Goldreich-Sridar law, which is indistinguishable from a Kolmogorov-spectrum in the isotropic average (Goldreich & Sridhar 1997). That means that a Kolmogorov-inertial range power law behaviour of hydrodynamical turbulence should also be found in the magnetic spectrum in any scenario.

⁸ Haugen et al. (2004) investigate numerically magnetic turbulence in the case of a Prandtl of order unity, and find a magnetic to turbulent energy ratio of the order of $f_B \approx 0.4$ in this regime. Since they report a $R_c \approx 35$, their case could be described by $d = 2.5$ dimensional magnetic intermittency. However, as Dennis & Chandran (2005) point out, the dissipation rate of turbulent energy seems to be doubled compared to not (or less) magnetised scenarios, which would lead to a reduction in the turbulent and magnetic energy densities by a similar factor. For the observables of the magnetic fields, like field strength, length, and Faraday signal, there would be very little numerical difference to the $d = 2$ scenario. For this reason, we do not follow this scenario separately, but assume it to be sub-summed under the $d = 2$ case.

- B. The average magnetic energy density ε_B is lower than the turbulent kinetic energy density ε_{kin} by $\varepsilon_B \approx \varepsilon_{\text{kin}} f_B$, where $f_B \sim R_c^{-(3-d)/2} \sim 0.05 \dots 0.2$ depending on the critical magnetic Reynolds number and the dimensionality of the magnetic structures.
- C. The magnetic fluctuations are concentrated on a perpendicular scale λ_B , which is smaller than the hydrodynamical turbulence injection scale λ_T by $\lambda_B \approx \lambda_T R_c^{1/2}$.
- D. Magnetic correlations exist up to a scale λ_T , turn there into an anti-correlation as a consequence of $\nabla \cdot \mathbf{B} = 0$, and quickly decay on larger scales.
- E. The fields may be spatially intermittent. This may be understood by Zeldovich's flux rope model, in which magnetic ropes with diameter λ_B are bent on scales of the order λ_T . Alternatively, also supported by recent numerical simulations, it can be understood in terms of magnetic sheets of thickness λ_B and size λ_T .
- F. In case of intermittent fields, the field strength within the magnetic structures should be in energy equipartition with the average turbulent kinetic energy density of their environment.
- G. The magnetic drag of such intermittent structures produces a hydrodynamical viscosity on large scales. In case of the Zeldovich-flux rope scenario, an estimate of a viscosity of 4% of the turbulent diffusivity $\kappa_T \approx v_T \lambda_T / 3$ was made by Longcope et al. (2003).

2.5. Observations

We investigate briefly if the above predictions of the non-helical dynamo theory are in agreement with observations.

- A. A Kolmogorov-like magnetic power spectrum in a cluster cool core is revealed by the Faraday rotation map of Hydra A (Vogt & Enßlin 2005).
- B. Translating the Faraday-rotation based estimate of the magnetic energy density to the expected turbulent energy density $\varepsilon_T \sim \varepsilon_B / f_B$ in the Hydra A cluster yields $0.3 \dots 1.0 \cdot 10^{-10} \text{ erg cm}^{-3}$, which corresponds to turbulent velocities of $v_{\text{turb}} \approx 250 \dots 430 \text{ km/s}$. This is comparable to velocities of buoyant radio plasma bubbles (Enßlin & Heinz 2002), which are expected to stir up turbulence (e. g. Churazov et al. 2001).
- C. The expected turbulence injection scale in the Hydra A cluster core is of the order of $\lambda_T \sim \lambda_B R_c^{1/2} \sim 10 \dots 20 \text{ kpc}$, again consistent with the radio plasma of Hydra A being the source of turbulence, since turbulence injection scale and the radio lobes of Hydra A have comparable dimensions. The dynamical connection of the radio source length scale and the magnetic turbulence scale would explain why the Faraday map of Hydra A is conveniently sized to show us the peak of the magnetic power spectrum (see Fig. 1).
- D. The expectation of weak magnetic fluctuations on scales larger than the turbulence injection scale is hard to test with the available data due to the limited size of the *RM* map used. However, the downturn of the magnetic power spectrum at small k -values visible in Fig. 1 is in good agreement

with the requirement of magnetic anti-correlations on large scales.

- E. Magnetic structures in form of flux ropes or ribbons might have been detected as stripy patterns in the *RM* map of 3C465 (Eilek & Owen 2002), and as polarised synchrotron filaments in the cluster radio relic in Abell 2256 (Clarke & Enßlin 2005), in support of the assumed intermittence of the small-scale dynamo .
- F. The fraction of strongly magnetised volume may be as small as $f_B = R_c^{-1} \approx 0.05 \dots 0.2$. Strongly intermittent fields in galaxy clusters may help to reconcile the discrepancy between Faraday and inverse Compton based magnetic field estimates (Enßlin et al. 1999). The latter estimate could easily be biased to low field regions due to the faster removal of ultra-relativistic electrons in strong field regions by synchrotron emission.
- G. The expected hydrodynamical viscosity on large scales in the Hydra cluster is of the order of $10^{28} \text{ cm}^2/\text{s}$ (if the estimate in Eq. 7 based on the flux rope picture is applicable). It is interesting to note, that Fabian et al. (2003b) argue for the comparable Perseus cluster cool core for a lower limit on the large scale viscosity of $4 \cdot 10^{27} \text{ cm}^2/\text{s}$. They base their arguments on the observation of very elongated H- α filaments which suggest a laminar flow pattern behind buoyantly rising radio bubbles. An upper limit on the viscosity in the (non-cooling core) Coma cluster of $\sim 3 \cdot 10^{29} \text{ cm}^2/\text{s}$ is reported by Schuecker et al. (2004). Both limits are consistent with our coarse estimate of the large scale viscosity and enclose it. However, it should be pointed out that the presence of a significant viscosity, as well as the underlying magnetic intermittency, in galaxy clusters should be regarded as being speculative, and not directly confirmed by observations. Nevertheless, there is a growing number of theoretical investigations⁹ on the possibility that viscosity helps to explain properties of the cluster gas.

3. Magneto-Hydrodynamical turbulence in cool cores

3.1. Scope of the approach

A theoretical model of the magneto hydrodynamical turbulence in cool cores of galaxy clusters is developed in the following. The model is intended to capture the most essential features of the physical picture. We do not attempt to make accurate numerical predictions, but hope to get insight into the scaling-relations of the different quantities and their order of magnitude values.

Although cool cores exhibit a structured gas distribution, for our order-of-magnitude calculation we describe them as quasi-homogeneous spheres. We briefly present a radial extension of our model in Sect. 3.7.

The episodic injection of radio plasma by the central galaxy into cool cores should lead to temporal variations of the state of

⁹ Pringle (1989); Churazov et al. (2001); Reynolds et al. (2002); Fujita et al. (2004); Ruszkowski et al. (2004); Dennis & Chandran (2005); Reynolds et al. (2005); Brüggen et al. (2005b); Kaiser et al. (2005)

the core. Nevertheless, we treat the system as being in a steady state. Our estimates provide therefore only approximate temporal mean values. Observations of cool cores will always show snapshots of the cool core evolution. Thus, deviations between our predictions and the observed state of individual cool cores should not be too surprising.

Detailed numerical modelling of the processes would be required to overcome our simplifying assumptions which is well beyond the scope of this initial investigation of the scenario presented.

3.2. A simplified cool core description

A cool core is a condensation of cold gas of mass M_{cc} , which dropped out of the hot phase of a galaxy cluster due to the faster radiative cooling of denser gas. The observables of the cool core, which can be used for diagnostics of the physical parameters, are the bolometric X-ray luminosity of the cool core L_{cc} , its temperature T_{cc} , and its radius r_{cc} from which the central electron density n_{cc} can be deduced.

The energy feedback of the central radio source prevents the cool core gas from falling below a characteristic temperature¹⁰ $T_{\text{cc}} \sim \text{keV}$, which is given by the requirement that the atomic line emission does not dominate. Otherwise, in the case of a lower temperature, the gas in the cool core would rapidly condense onto the central galaxy due to a cooling catastrophe driven by emission-lines. The pressure in a cool core is

$$P_{\text{cc}} = 2 n_{\text{cc}} T_{\text{cc}}, \quad (8)$$

where we ignore here and in the following the presence of any element heavier than Hydrogen in pressure and mass terms for simplicity. The cool core gas mass is therefore

$$M_{\text{cc}} = n_{\text{cc}} m_{\text{p}} V_{\text{cc}}, \text{ where } V_{\text{cc}} = \frac{4\pi}{3} r_{\text{cc}}^3. \quad (9)$$

The X-ray luminosity of the cool core is given by

$$L_{\text{cc}} = \Lambda_{\text{X}}(T_{\text{cc}}) n_{\text{cc}}^2 V_{\text{cc}}, \quad (10)$$

where

$$\Lambda_{\text{X}}(T_{\text{cc}}) = \Lambda_0 T_{\text{cc}}^{\frac{1}{2}} + \Lambda_{\text{lines}}(T_{\text{cc}}) \quad (11)$$

consists of a Bremsstrahlung- and a line emission term. The line emission term should be at best comparable to the Bremsstrahlung-term, since otherwise the full core would run into a cooling catastrophe. Therefore, we can ignore the line-term in our rough estimate

$$\Lambda_{\text{X}}(T_{\text{cc}}) \approx \Lambda_0 T_{\text{cc}}^{\frac{1}{2}}, \quad (12)$$

with $\Lambda_0 = 5.96 \cdot 10^{-24} \text{ erg s}^{-1} \text{ cm}^3 \text{ keV}^{-1/2}$ (assuming a metalicity of 0.3 solar).

¹⁰ We express temperatures in terms of energies by setting the Boltzman constant to unity ($k_{\text{B}} = 1$)

3.3. Hydrodynamical turbulence injection

We assume that the injection from radio galaxies is the dominant heating mechanism. Although radio galaxies certainly inject energy not all of this is in form of turbulence. During the very initial phase of inflation of a radio bubble there are shocks, which can heat the environment (Heinz et al. 1998; Fabian et al. 2003a). Later on, a series of sound waves are produced, which might be dissipated through viscosity in the medium¹¹. In any case, when a radio bubble raises buoyantly in the cool core atmosphere, the environmental gas is flowing around it, which leads to injection of kinetic energy from the central radio galaxy into the cool core. The time averaged turbulence power of the source is

$$L_{\text{T}} = f_{\text{T}} L_{\text{cc}} = \eta_{\text{T}} L_{\text{rg}}, \quad (13)$$

where f_{T} is the fraction of cool core heating done by turbulence, $\eta_{\text{T}} \leq 1$ is the efficiency of kinetic energy transfer between the injected radio plasma and the cool core gas, and L_{rg} is the mechanical luminosity of the radio galaxy ($P dV$ work per time). Churazov et al. (2002) argue that the efficiency factor η_{T} should be of the order one since the radio plasma looses most of its energy by adiabatic expansion during its buoyant rise through one scale-height of the cluster atmosphere. This energy is transferred mechanically to the kinetic energy of the ICM gas and is finally dissipated into heat. It is controversial if most of this energy is dissipated within the cool core, or within the outer regions of the cluster. Here, we assume the former and set $\eta_{\text{T}} = f_{\text{T}} = 0.5$ allowing also non-turbulent heating (shock waves, sound waves, heat transport). However, we also provide the scaling of our results with these parameters.

The injected kinetic energy is dissipated through a Kolmogorov-cascade within an eddy turnover-time

$$\tau_{\text{T}} \sim \lambda_{\text{T}} / v_{\text{T}}, \quad (14)$$

where λ_{T} and v_{T} are the turbulence injection scale and turbulence root mean square velocity, respectively. The average turbulent energy of the cool core $E_{\text{T}} = M_{\text{cc}} v_{\text{T}}^2 / 2$ is therefore

$$E_{\text{T}} = L_{\text{T}} \tau_{\text{T}} \approx f_{\text{T}} L_{\text{cc}} \lambda_{\text{T}} / v_{\text{T}}, \quad (15)$$

yielding

$$\frac{v_{\text{T}}^3}{\lambda_{\text{T}}} = \frac{2 f_{\text{T}} L_{\text{cc}}}{M_{\text{cc}}} = \frac{2 f_{\text{T}} L_{\text{cc}}}{m_{\text{p}} n_{\text{cc}} V_{\text{cc}}}. \quad (16)$$

This would allow the determination of the turbulent velocity and energy density if the turbulent injection scale were known. In the following, we attempt a rough estimate of the expected turbulent length scale λ_{T} .

3.4. Hydrodynamical turbulence injection scale

In the picture adopted for this work, the turbulence is stirred by the movement of buoyant radio plasma bubbles. The turbulence

¹¹ Pringle (1989); Churazov et al. (2001); Reynolds et al. (2002); Fujita et al. (2004); Ruszkowski et al. (2004); Dennis & Chandran (2005)

injection scale should therefore be of the order of the radius r_{bub} of the bubbles, which we approximate to be spheres. Assuming an ultra-relativistic equation of state for the radio plasma, we find the volume of the bubble is given as

$$V_{\text{bub}} = E_{\text{bub}}/(4P), \quad (17)$$

where

$$E_{\text{bub}} = L_{\text{rg}} \tau_{\text{bub}}/2 = f_{\text{T}} L_{\text{cc}} \tau_{\text{bub}}/(2\eta_{\text{T}}) \quad (18)$$

is the mechanical energy released by the radio galaxy into a bubble during the time τ_{bub} the bubble needs to leave the cool core buoyantly. If the turbulence stirring bubbles were filled mostly by thermal gas, the volume of the bubble would be $V_{\text{bub}} = 2E_{\text{bub}}/(5P)$, which would make some difference to our estimates, but none which is changing the order of magnitude of our results.

The time available for the jets to inflate the bubble is its rise time through the cool core

$$\tau_{\text{bub}} \sim \frac{r_{\text{cc}}}{v_{\text{bub}}} \sim \left(\frac{r_{\text{cc}}}{r_{\text{bub}}} \right)^{\frac{1}{2}} \frac{r_{\text{cc}}}{2c_s}, \quad (19)$$

and can be estimated from the balance of drag and buoyance forces (e.g. Enßlin & Heinz 2002).

Combining Eq. 17, 18, and 19 yields the bubble radius

$$r_{\text{bub}} = \left(\frac{3f_{\text{T}} L_{\text{cc}} r_{\text{cc}}^{3/2}}{64\pi\eta_{\text{T}} c_s P_{\text{cc}}} \right)^{\frac{2}{7}}, \quad (20)$$

and thereby the required hydrodynamical turbulence scale $\lambda_{\text{T}} \sim r_{\text{bub}}$. Using this and the derived relations above, the turbulent velocity calculates as

$$\begin{aligned} v_{\text{T}} &= \frac{3^{\frac{1}{21}} \eta_{\text{T}}^{\frac{1}{3}} \Lambda_0^{\frac{3}{7}} n_{\text{cc}}^{\frac{3}{7}} r_{\text{cc}}^{\frac{3}{7}} T_{\text{cc}}^{\frac{1}{14}}}{2^{\frac{4}{21}} 5^{\frac{1}{21}} f_{\text{T}}^{\frac{1}{3}} m_{\text{p}}^{\frac{2}{7}}} \\ &= 173 \text{ km/s} \left(\frac{\eta_{\text{T}}}{f_{\text{T}}} \right)^{\frac{1}{3}} \left(\frac{n_{\text{cc}}}{0.1 \text{ cm}^{-3}} \right)^{\frac{3}{7}} \left(\frac{r_{\text{cc}}}{10 \text{ kpc}} \right)^{\frac{3}{7}} \left(\frac{T_{\text{cc}}}{\text{keV}} \right)^{\frac{1}{14}}, \end{aligned} \quad (21)$$

and thus, the turbulent energy density is given by

$$\varepsilon_{\text{T}} = \frac{3^{\frac{2}{21}} \eta_{\text{T}}^{\frac{2}{3}} \Lambda_0^{\frac{6}{7}} m_{\text{p}}^{\frac{3}{7}} n_{\text{cc}}^{\frac{13}{14}} r_{\text{cc}}^{\frac{6}{7}} T_{\text{cc}}^{\frac{1}{7}}}{2^{\frac{29}{21}} 5^{\frac{2}{21}} f_{\text{T}}^{\frac{2}{3}}}. \quad (22)$$

For a number of prominent cool core clusters, Tab. 1 contains the values for v_{T} , $\lambda_{\text{T}} = r_{\text{bub}}$, and ε_{T} as expected from our steady-state description of cool core turbulence. Deviations due to episodic evolution of cool core turbulence are possible and expected.

3.5. Magnetic turbulence

The energy density of the magnetic turbulence ε_B is lower by a factor $f_B \sim 0.05 \dots 0.2$ than the kinematic one ε_{T} . The length-scale is also smaller by a factor $R_{\text{c}}^{-1/2}$. The root-mean-square magnetic field strength in the cool core is therefore given by

$$B_{\text{rms}} = \sqrt{8\pi\varepsilon_{\text{T}}f_B} = \frac{2^{\frac{17}{21}} 3^{\frac{1}{21}} \pi^{\frac{1}{2}} \eta_{\text{T}}^{\frac{1}{3}} \Lambda_0^{\frac{3}{7}} m_{\text{p}}^{\frac{3}{14}} n_{\text{cc}}^{\frac{13}{14}} r_{\text{cc}}^{\frac{3}{7}} T_{\text{cc}}^{\frac{1}{14}}}{5^{\frac{1}{21}} f_{\text{T}}^{\frac{1}{3}} R_{\text{c}}^{\frac{3}{4}}} \quad (23)$$

$$= \begin{cases} 5.6 \mu\text{G} \left(\frac{\eta_{\text{T}}}{f_{\text{T}}} \right)^{\frac{1}{3}} \left(\frac{n_{\text{cc}}}{0.1 \text{ cm}^{-3}} \right)^{\frac{13}{14}} \left(\frac{r_{\text{cc}}}{10 \text{ kpc}} \right)^{\frac{3}{7}} \left(\frac{T_{\text{cc}}}{\text{keV}} \right)^{\frac{1}{14}} \left(\frac{R_{\text{c}}}{20} \right)^{-\frac{1}{2}} \\ 10 \mu\text{G} \left(\frac{\eta_{\text{T}}}{f_{\text{T}}} \right)^{\frac{1}{3}} \left(\frac{n_{\text{cc}}}{0.1 \text{ cm}^{-3}} \right)^{\frac{13}{14}} \left(\frac{r_{\text{cc}}}{10 \text{ kpc}} \right)^{\frac{3}{7}} \left(\frac{T_{\text{cc}}}{\text{keV}} \right)^{\frac{1}{14}} \left(\frac{R_{\text{c}}}{35} \right)^{-\frac{1}{2}} \end{cases}$$

in our flux rope ($d = 1$) and magnetic sheet ($d = 2$) scenarios, respectively. The magnetic autocorrelation length is

$$\begin{aligned} \lambda_B &= \frac{\lambda_{\text{T}}}{R_{\text{c}}^{\frac{1}{2}}} = \frac{3^{\frac{1}{7}} \Lambda_0^{\frac{2}{7}} m_{\text{p}}^{\frac{1}{7}} n_{\text{cc}}^{\frac{2}{7}} r_{\text{cc}}^{\frac{9}{7}}}{2^{\frac{11}{7}} 5^{\frac{1}{7}} R_{\text{c}}^{\frac{1}{2}} T_{\text{cc}}^{\frac{2}{7}}} \\ &= 0.53 \text{ kpc} \left(\frac{n_{\text{cc}}}{0.1 \text{ cm}^{-3}} \right)^{\frac{2}{7}} \left(\frac{r_{\text{cc}}}{10 \text{ kpc}} \right)^{\frac{9}{7}} \left(\frac{T_{\text{cc}}}{\text{keV}} \right)^{-\frac{2}{7}} \left(\frac{R_{\text{c}}}{20} \right)^{-\frac{1}{2}} \end{aligned} \quad (24)$$

3.6. Predicting an observable: RM dispersion

Knowing the depth of the Faraday screen r_{cc} , the magnetic field strength $\langle B^2 \rangle$, and the magnetic autocorrelation length λ_B allows to predict the expected dispersion of the Faraday rotation measure from a central radio source¹², assuming an isotropic distribution of magnetic field strengths with the help of Eq. 40 of Enßlin & Vogt (2003):

$$\langle RM^2 \rangle = \frac{1}{2} a_0^2 n_{\text{cc}}^2 r_{\text{cc}} \lambda_B \langle B^2 \rangle \quad (25)$$

$$= \frac{3^{\frac{5}{21}} \pi a_0^2 \eta_{\text{T}}^{\frac{2}{3}} \Lambda_0^{\frac{8}{7}} m_{\text{p}}^{\frac{4}{7}} n_{\text{cc}}^{\frac{29}{21}} r_{\text{cc}}^{\frac{22}{7}}}{2^{\frac{20}{21}} 5^{\frac{5}{21}} f_{\text{T}}^{\frac{2}{3}} R_{\text{c}}^{2-\frac{d}{2}} T_{\text{cc}}^{\frac{1}{7}}} \quad (26)$$

$$RM_{\text{rms}}^{\text{exp}} = \begin{cases} \frac{739}{\text{m}^2} \left(\frac{\eta_{\text{T}}}{f_{\text{T}}} \right)^{\frac{1}{3}} \left(\frac{n_{\text{cc}}}{0.1 \text{ cm}^{-3}} \right)^{\frac{29}{14}} \left(\frac{r_{\text{cc}}}{10 \text{ kpc}} \right)^{\frac{11}{7}} \left(\frac{T_{\text{cc}}}{\text{keV}} \right)^{-\frac{1}{14}} \left(\frac{R_{\text{c}}}{20} \right)^{-\frac{3}{4}} \\ \frac{1180}{\text{m}^2} \left(\frac{\eta_{\text{T}}}{f_{\text{T}}} \right)^{\frac{1}{3}} \left(\frac{n_{\text{cc}}}{0.1 \text{ cm}^{-3}} \right)^{\frac{29}{14}} \left(\frac{r_{\text{cc}}}{10 \text{ kpc}} \right)^{\frac{11}{7}} \left(\frac{T_{\text{cc}}}{\text{keV}} \right)^{-\frac{1}{14}} \left(\frac{R_{\text{c}}}{35} \right)^{-\frac{1}{2}} \end{cases}$$

The two cases correspond to filamentary and sheet like magnetic structure scenarios, respectively. Here, $a_0 = e^3/(2\pi m_e^2 c^4)$ is the usual Faraday rotation constant¹³.

It is worth noting that the scaling of the Faraday dispersion, which can approximately be written as $RM_{\text{rms}}^{\text{exp}} \propto n_{\text{cc}}^2 r_{\text{cc}}^{3/2} T_{\text{cc}}^0$, is sufficiently similar to that of the bolometric luminosity of the cool core $L_{\text{cc}} \propto n_{\text{cc}}^2 r_{\text{cc}}^3 T_{\text{cc}}^{1/2}$ and also to the mass deposition rate $\dot{M} \propto L_{\text{cc}}/T_{\text{cc}} \propto n_{\text{cc}}^2 r_{\text{cc}}^3 T_{\text{cc}}^{-1/2}$ to expect significant correlations, which are indeed observed (e.g. Taylor et al. 2002).

¹² Background sources should have twice the variance $\langle RM^2 \rangle$ given here due to the doubled screen depth.

¹³ Eq. 25 differs from the usually used, but inaccurate RM dispersion formula, which is based on the cell model for the magnetic fields

$$\langle RM^2 \rangle \approx \frac{1}{3} a_0^2 n_{\text{cc}}^2 r_{\text{cc}} \lambda_{\text{RM}} \langle B^2 \rangle$$

First, the proper magnetic autocorrelation length λ_B is used in Eq. 25, which differs in a non-trivial way – since this is magnetic power-spectrum dependent – from the RM autocorrelation length λ_{RM} derived from RM maps. Usually, $\lambda_{\text{RM}} > \lambda_B$. Second, the numerical factor $\frac{1}{2}$ in Eq. 25 takes properly account for the effect of the constraint $\nabla \cdot \mathbf{B} = 0$, whereas for the above Eq., uncorrelated patches with internally constant magnetic fields were assumed, which do not have $\nabla \cdot \mathbf{B} = 0$ at the patch boundaries. Due to the differences, published magnetic field values based on the above Eq. does not need to be accurate, although the two errors partly compensate each other.

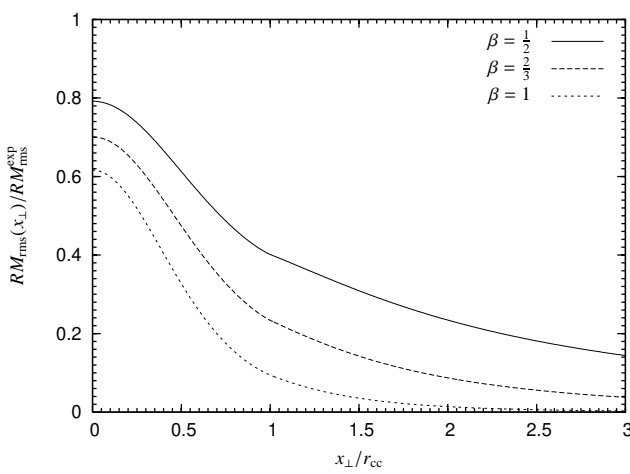


Fig. 2. Radial profile of the expected RM dispersion for a line of sight starting in the midplane of a β -profile cool core, but being displaced from the cluster centre by x_{\perp} . The RM dispersion is given in units of our result $RM_{\text{rms}}^{\text{exp}}$ in Eq. 25 for the solid sphere model of the cool core.

3.7. Approximate treatment of the cool core structure

In the following, we generalise the simplified geometry of a homogeneous cool core to one which has a radial structure. This generalisation allows us to predict the radial dependence of the various quantities and to test if our predictions of the central RM dispersion are expected to change significantly due to the contribution from radii outside the cool core radius.

In order to provide a radial dependent geometry, we make an additional assumption about the radial balance between heating and cooling. We assume that the cool core is settled in an hydrodynamical state, where heating and cooling are balanced locally at all radii below the cooling radius. Note that this does not necessarily need to be true, since in a convecting system the location of heat deposition and radiative cooling can differ, but for the sake of simplicity, we use this approximation.

The cool core is divided into spherical shells of thickness dr , which have a volume $dV(r) = 4\pi r^2 dr$ and a luminosity $dL(r) = \Lambda_X(T_{\text{cc}}) n_{\text{cc}}^2 dV(r)$. Our arguments about the balance of turbulent heating and radiative cooling made in Sect. 3.3 can be identically applied to each of these shells individually, leading to a relation equivalent to Eq. 16:

$$\frac{v_T^3(r)}{\lambda_T(r)} = \frac{2 f_T}{m_p n_{\text{cc}}} \frac{dL}{dV}(r). \quad (27)$$

To derive the local turbulence injection scale, we use again the local characteristic buoyancy time $\tau_{\text{bub}}(r) \sim r/v_{\text{bub}}(r)$ to predict the bubble size at any cluster radius $r > r_{\text{cc}}$. For $r \leq r_{\text{cc}}$, we use r_{cc} to treat the central flat density profile properly. In doing so, we find that the replacement

$$r_{\text{cc}} \rightarrow \max(r_{\text{cc}}, r) \quad (28)$$

in any former equation describing local properties as in Eqs. 20-25 gives the appropriate function of radius r . Of special interest may be the expected radial scaling of the typical

magnetic field strength: $B_{\text{rms}} \propto n_e^{13/14}(r) r^{3/7}$ which is usually a decreasing function of the radius due to the steepness of the electron profiles. For example for $n_e \propto r^{-2}$ (and $T(r) \approx \text{const}$) we find $B_{\text{rms}} \propto r^{-10/7} \propto n_e^{5/7}$ which lies well within the range of usually assumed magnetic field scaling with electron density $B_{\text{rms}} \propto n_e^{0.5 \dots 1}$ (e.g. Dolag et al. 2001).

Global quantities like the energy content, the luminosity of a volume, etc. are calculated by performing the appropriate volume integrals. The increase of the Faraday dispersion along the line of sight should therefore be given by the differential analogy to Eq. 25

$$\frac{d\langle RM^2 \rangle}{dl} = \frac{1}{2} a_0^2 n_{\text{cc}}^2 \lambda_B \langle B^2 \rangle \quad (29)$$

$$= \frac{3^{5/21} \pi a_0^2 \eta_T^{2/3} \Lambda_0^{8/7} m_p^{4/7} n_e^{29/7}(r) \max^{15/7}(r_{\text{cc}}, r)}{2^{20/21} 5^{5/21} f_T^{2/3} R_c^{2-4/7} T_e^{1/7}(r)}, \quad (30)$$

which reduces to the former result given by Eq. 26 if integrated over a cool core sphere with constant properties within r_{cc} .

Eq. 30 allows us to check under which conditions our constant core model gives appropriate results, and under which conditions the RM contributions from larger radii become essential.

For an electron density profile described by the usual β -model,

$$n_e(r) = n_{\text{cc}} \left(1 + \frac{r^2}{r_{\text{cc}}^2}\right)^{-\frac{3}{2}\beta}, \quad (31)$$

we find that the contribution to the RM dispersion per logarithmic radius peaks around the core radius r_{cc} if $\beta > 0.25$ (a similar statement can be made for the cool core dominating the X-ray emissivity if $\beta > 0.5$). Since typical cluster electron density profiles are described by $\beta \geq 0.5$, our ignorance of contributions of outer regions to the RM dispersion only introduces a moderate error of the order of 20–40% (depending on β) for line of sights starting in the cluster centre. Off-centre line-of-sights, which often occur for extended radio lobes in our sample, will result in significantly lower RM dispersions. This can be seen in Fig. 2, where numerically estimated RM -profiles are shown.

We note that typical pairs of radio lobes are not located in the midplane of the cluster. One lobe has a shorter and one has a longer line-of-sight through the Faraday-active medium. In a spherical geometry of the cluster gas, the additionally accumulated $\langle RM^2 \rangle$ of the back lobe, and the missing of the front lobe should compensate roughly in an average over both lobes, provided both lobes are in mirror symmetric positions with respect to the cluster centre. Therefore, in such a case the midplane RM dispersion is a good reference point.

4. Application to Cool Cores

In the following, we apply our model to a number of cool core clusters. The input parameters of our calculations are the central electron density n_{cc} , the central gas temperature T_{cc} , and the core radius r_{cc} of the cool core. The numbers are taken from

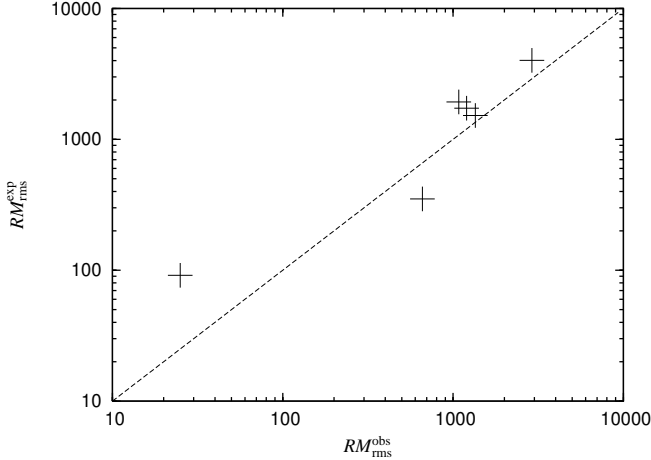


Fig. 3. Comparison of observed (cross) and theoretically expected (case $d = 1, R_c = 20$) (dashed line) root-mean-squared RM signal. Note, that the expected RM is calculated for a radio source located at the centre of the cluster, whereas most RM measurements are somewhat off centre, probably leading to a reduced observed signal.

the literature and the corresponding references are given in the sections referring to individual clusters in the Appendix A, together with detailed discussions of the individual datasets. The cluster parameters and the derived properties are summarised in Tab. 1.

As a consistency check for the used radii of the cool cores, we calculate the emissivity L_{cc} within the cool core according to Eq. 10 and compare this to the reported bolometric X-ray luminosity of the complete cluster L_{cluster} . The fraction of X-ray luminosity which is due to the cool core is in the range of $L_{cc}/L_{\text{cluster}} = 1\% - 50\%$. The typical fractional luminosity within the cooling radius, which is defined by the gas having a cooling time less than the Hubble time, was estimated by Peres et al. (1998). Since the cooling radius is larger than the core radius of the cool core a systematic difference is expected, and indeed found since $L(< r_{\text{cooling}})/L_{\text{cluster}} = 40\% - 60\%$ according to Peres et al. (1998). The large differences for some clusters between the ratios are due to shallow electron density profiles with $\beta \approx 0.5$ (see Sect. 3.7).

The other quantities in Tab. 1 are calculated according to the formulae given in Sect. 3. Note that our expected $RM_{\text{rms}}^{\text{exp}}$ is calculated for a polarised synchrotron source in the middle of the cool core, whereas the real radio emitting volume may be displaced due to an inclination between radio jet and line-of-sight, and/or due to a non-central position. This will cause some deviation of our expectations from the observations and usually biases the observational values to be lower.

For a sample of cool cores with luminosities between $10^{43} - 10^{45}$ erg/s, we predict turbulent velocities in the range 100 – 300 km/s, magnetic field strengths in the range 3 – 13 μG ($1-d$ scenario) or 6 – 23 μG ($2-d$ scenario), and Faraday dispersions in the range 100 – 4000 m^{-2} (150 – 6000 in the $2-d$ scenario). These values should be compared to existing Faraday rotation measurements, field strength estimates, and future X-

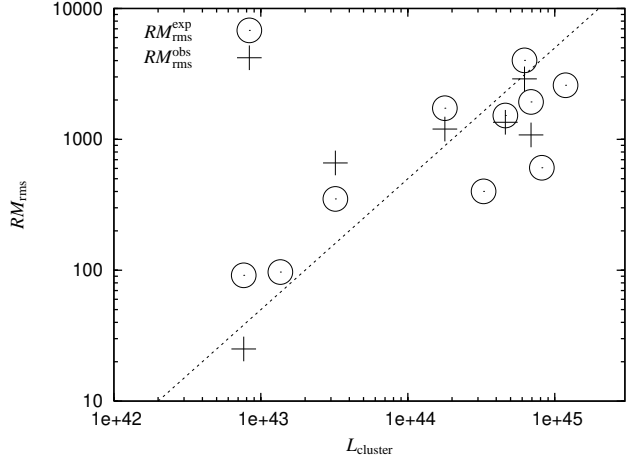


Fig. 4. Expected (case $d = 1, R_c = 20$) and observed RM dispersion values versus the bolometric cluster luminosity. A linear correlation is also shown to guide the eye.

ray-spectroscopically determined velocity dispersions, as done in Tab. 1, and Figs. 3 & 4. We further list our expectations for the large-scale magnetic viscosity, which we like to be regarded as speculative, and which were estimated using the calculations of Longcope et al. (2003) for an assumed $1-d$ flux-rope picture of the magnetic field configuration.

To summarise our results, we find that both, the one and two dimensional scenarios for the magnetic structures, predict rotation measures which are of the same order of magnitude as the observed ones. In cases where observational estimates for field strength and length scales existed, there is also a better than order of magnitude agreement. The explosive dynamo seems to underpredict the observed Faraday rotation by a factor of two, due to the shorter magnetic length scale predicted. In general, we would not expect our model to be more accurate than to within a factor of two. This is especially true for our rough parametrisation of the saturation state of the explosive dynamo.

5. Conclusion

We showed that many properties of magnetic field measurements in cool core clusters, and especially in the case of Hydra A, which we investigate in detail, seem to support the picture that a saturated small-scale turbulent dynamo is maintaining the magnetic fields. Although there exist dramatic differences between small-scale dynamo scenarios, their saturated state might be quite similar. If it can be assumed to be mostly a balance between the turbulent entangling and Alfvénic straightening of magnetic field lines, the state is characterised by only two numbers: the effective dimensionality of the magnetic structures and the ratio between turbulence injection scale and magnetic correlation length. Casting three representative small-scale dynamo descriptions into this formulation, we find that they are all in rough agreement with the data, which is as much as we can expect given the approximate nature of our treatment. The investigated scenarios are the *flux rope dy-*

cluster properties	Hydr.	Cent.	Cygn.	A1958	A2597	3C31	Pers.	A85	A2199	Virgo
n_{cc} [10 ⁻³ /ccm]	56.1	80.6	153	189	73.5	180	50.8	30.8	33.7	151
T_{cc} [keV]	2.7	2.2	6.5	3.7	1.3	0.7	3	5.5	1.6	1
r_{cc} [kpc]	35.5	8.57	10.7	13.4	28	1.2	57	45	29	1.6
RM_{rms}^{obs} [m ⁻²]	1350	660	1200	2900	1080	25	—	—	—	—
$L_{cluster}$ [10 ⁴⁴ erg/s]	4.61	0.32	1.79	6.22	6.89	0.077	11.8	8.16	3.28	0.14
$L(< r_{cooling})/L_{cluster}$	0.52	0.41	0.49	—	0.61	—	0.59	0.3	0.47	0.5
$L_{cc}/L_{cluster}$	0.37	0.14	0.3	0.2	0.14	0.0045	0.51	0.18	0.078	0.005
hydrodynamical turbulence										
$\lambda_B \sim r_{bub}$ [kpc]	7.68	1.45	1.7	2.84	7.52	0.2	13.3	7.15	5.94	0.25
ε_T [10 ⁻¹⁰ erg/ccm]	0.29	0.16	0.76	1.27	0.35	0.12	0.37	0.13	0.089	0.11
v_T [km/s]	250	156	244	283	240	87.5	295	225	177	94
magnetic turbulence										
λ_B [kpc]	1.72	0.32	0.38	0.64	1.68	0.045	2.97	1.6	1.33	0.056
B_{rms} [μ G]	6.06	4.55	9.78	12.6	6.68	3.8	6.82	4.04	3.34	3.74
κ_{visc} [10 ²⁷ cm ² /s]	7.89	0.93	1.71	3.31	7.43	0.073	16.1	6.61	4.33	0.097
RM_{rms}^{exp} [m ⁻²]	1520	351	1730	4010	1930	91.5	2590	607	400	96.9
$RM_{rms}^{obs}/RM_{rms}^{exp}$	0.89	1.88	0.69	0.72	0.56	0.27	—	—	—	—
magnetic turbulence										
λ_B [kpc]	1.3	0.25	0.29	0.48	1.27	0.034	2.25	1.21	1	0.042
B_{rms} [μ G]	11.1	8.36	18	23.2	12.3	6.99	12.5	7.44	6.13	6.88
RM_{rms}^{exp} [m ⁻²]	2430	561	2770	6420	3090	146	4140	970	640	155
$RM_{rms}^{obs}/RM_{rms}^{exp}$	0.55	1.18	0.43	0.45	0.35	0.17	—	—	—	—
magnetic turbulence										
$d = 2 R_c = R_c^*$ – explosive dynamo										
R_c	1060	461	461	922	1630	308	1380	541	839	279
λ_B [kpc]	0.24	0.068	0.079	0.094	0.19	0.012	0.36	0.31	0.2	0.015
B_{rms} [μ G]	4.75	4.39	9.44	10.3	4.7	4.06	5	3.75	2.77	4.09
RM_{rms}^{exp} [m ⁻²]	443	155	762	1250	452	49.3	659	247	131	54.9
$RM_{rms}^{obs}/RM_{rms}^{exp}$	3.04	4.27	1.57	2.32	2.39	0.51	—	—	—	—

Table 1. Application of the model to cool cores of the Hydra A (Hydr.), Centaurus (Cent.), Cygnus A (Cygn.), A1985, A2597, 3C31, Perseus (Pers.), A85, A2199 and Virgo clusters of galaxies. The first part of the table contains the cluster parameters whose values were taken from the literature. References and comments on possible biases of the data are given in Sect. 4 and in detail in Appendix A. The second part describes the expected hydrodynamical turbulence. The third, fourth, and fifth parts describe the expected magnetic turbulence for the scenarios of magnetic flux ropes ($d = 1, R_c = 20$), flux sheets ($d = 2 R_c = 35$), and flux sheets in the explosive dynamo scenario ($d = 2 R_c = R_c^*$), respectively. Numbers are given here to three digits accuracy, irrespective the fact that the real uncertainties of most quantities are much larger.

namo (e.g Zeldovich et al. 1990; Subramanian 1999, with a renormalised Reynolds number), the *fluctuation dynamo* as described in Subramanian et al. (2006), and the *explosive dynamo* introduced by Schekochihin et al. (2005).

The likely energy source of the expected turbulence are buoyant radio bubbles from the central galaxy, which can inject turbulence with the right amount of power, and also on length-scales, which fit to the observed magnetic correlation scales well.

Motivated by these indications of the physical processes in cool core clusters, we developed a steady state scenario for the hydrodynamical and magnetic turbulence, assuming that the turbulent feedback from the central radio source compensates for the cool core radiative losses. This scenario predicts turbulent length scales and energy densities which can be compared to observations.

The hydrodynamical turbulence could have been probed with the Astro-E2 satellite mission which unfortunately failed. We hope that successor missions will permit the determination of the gas velocity dispersion (Sunyaev et al. 2003; Inogamov & Sunyaev 2003; Brüggen et al. 2005a). At present,

the magnetic turbulence can be tested due to the existing Faraday rotation measurements of extended radio sources in cool core clusters. The Faraday dispersion is a combined measure of the magnetic field strength and correlation length.

For a sample of prominent cool core clusters, we calculate the expected hydro- and magnetic-turbulence, and the predicted Faraday dispersion. In cases of existing Faraday measurements, we find that our estimates reproduce the observed magnitude of the dispersion over roughly two orders of magnitude in RM (or four in $\langle RM^2 \rangle$). On average, our predictions for the models based on the *flux rope* and the *fluctuating dynamo* (Subramanian 1999; Subramanian et al. 2006) are a factor of two higher than the measurements, which is not too surprising, since the actual data sample larger cluster radii, whereas our estimates are aiming for a radio source at the cluster centre. The predictions for the Faraday dispersion in the *explosive dynamo* scenario are a factor of two below the observation as shown by Schekochihin & Cowley (2006), which is a bit more severe, since geometrical considerations will only enlarge this discrepancy. However, it should be acknowledged that the description of the saturated state of this dynamos is currently more an ed-

ucated guess than a precise estimate. Thus, also this model should be regarded to be in agreement with the data.

The critical reader might wonder about the amount of fine tuning which went into our model. The answer is nearly none, but this is probably a mere coincidence rather than a prove for the investigated scenario. There are various places in the calculation where factors of order one could or should have been introduced. One example is the assumption of the bubble radius being exactly the turbulence injection scale. This assumption will require verification by numerical simulations of the hydrodynamics, which is well beyond the scope of this initial investigation. Another uncertain area are the adopted parameters of the dynamo theory, which are also not fully settled in the literature.

Nevertheless, we have shown that the straight-forward application of current concepts of turbulent magnetic dynamos in combination with the emerging picture of cool core stabilisation via heat injection due to the dissipation of turbulence seeded by radio galaxy feedback leads to expectations for the Faraday rotation signal which match well with the observed ones. This is the case for a variety of galaxy clusters spanning two orders of magnitude in their X-ray luminosities. Therefore, our picture of cluster cool core heating by radio galaxy feedback in combination with generic ideas about the properties of the saturated state of non-helical, small scale magnetic dynamos passed a critical test. Our scenario provides a number of testable predictions, especially about the level of fluid turbulence in individual clusters. We hope that future measurements of the plasma properties in galaxy clusters will even permit discrimination between the different small-scale dynamo models.

Acknowledgements. We acknowledge stimulating discussions with K. Subramanian and A. Schekochihin on the theory of small-scale dynamos. We are thankful to R. Laing to provide us with the results on 3C31 prior to publication, and to V. Springel and E. Churazov for comments on the manuscript.

Appendix A: Individual clusters

In this Appendix the observational data is discussed. Note, this collection of literature values for cool core cluster parameters made use of the work done by Pfrommer & Enßlin (2004a).

A.1. Hydra A cluster

The gas parameters for the Hydra A cluster are taken from Mohr & Evrard (1997), and the X-ray luminosity is provided by Ikebe et al. (1997). The first detailed *RM* map of Hydra A was published by Taylor & Perley (1993), which exhibited very large *RM* values, especially for the south lobe of Hydra A. The data was reanalysed using the PACERMAN algorithm (Dolag et al. 2005; Vogt et al. 2005), which removed all areas in the northern-lobe, and many of the southern-lobe with extremely high *RM* values, indicating that those were observational artefacts. Since the southern lobe *RM* data seem to be still contaminated by observational artefacts, as statistical tests for anti-correlations of gradients of polarisation angles and *RM* values reveal (Enßlin et al. 2003), we use only the dispersion

of the northern lobe, as reported by Vogt et al. (2005). The same *RM* map was analysed by Vogt & Enßlin (2005) using a maximum-likelihood power spectra estimator (see Fig. 1), revealing central magnetic field strength of $B_{\text{rms}} \approx 7 \mu\text{G}$ with an autocorrelation length of $\lambda_B \approx 3 \text{ kpc}$.

We note that model expectations and observational values of Faraday dispersion, magnetic field strength, and autocorrelation length agree well. Since the Hydra A north lobe is known to approach the observer (and the radio emission extend to larger radii), the observational *RM* dispersion should be a bit biased to lower values.

A.2. Centaurus cluster

The central electron density and the cool core radius are taken from Mohr et al. (1999)¹⁴, and the central temperature from White (2000)¹⁵. The observed Faraday dispersion for the Centaurus cluster is derived from the embedded radio source PKS 1246-410 by Taylor et al. (2002). The published Faraday rotation map reveals several isolated patches of extreme *RM* values, and a histogram of *RM* values exhibits multiple peaks. A statistical analysis of the alignment of *RM* gradients and polarisation angle gradients reveals a significant anti-correlation between the two (Enßlin et al. 2003), which is also an indication of observational artefacts in this map. Thus, the reported *RM* dispersion may be too large. However, an order of magnitude agreement between observed and expected *RM* dispersion is found.

Taylor et al. (2002) report a *RM*-correlation length of $\lambda_{RM} \sim 0.7 \text{ kpc}$ and a field strength of $9 \mu\text{G}$, which is significantly different from our expectations. The different length scale is not surprising, since usually $\lambda_{RM} > \lambda_B$ (Enßlin & Vogt 2003). The larger observationally derived magnetic field strength may be a result of the very small core radius and/or the possible overestimate of the *RM* dispersion reported in Taylor et al. (2002).

To summarise, the X-ray and radio observational data of the cool core of the Centaurus cluster would need further improvements before conclusive statements about an agreement or disagreement of our model and observations can be made in this case. Both, the observed and the expected *RM* dispersion could be subject to re-adjustments. We like to stress that the complex morphology of this cool core is probably causing the difficulties to single out a ‘*real*’ core radius and central electron density.

¹⁴ Using the extremely small core radius given in Taylor et al. (2002) leads to a cool core fractional luminosity of only 3%, which is obviously much smaller than the 40% observed (Peres et al. 1998).

¹⁵ Lower central temperatures have been reported by Sanders & Fabian (2002) and Taylor et al. (2002), but since they were not used for the electron density estimates, and since our magnetic field and *RM* predictions are quite insensitive to the temperature, we do not use them.

A.3. Abell 1958 cluster (3C295)

The electron density, central temperature, cool core radius, and dispersion measure are taken from Allen et al. (2001) and the cluster luminosity from Allen et al. (2003).

The agreement of predicted and observed Faraday dispersion is very good. Furthermore, the rather high predicted magnetic field strength of $10 - 20 \mu\text{G}$ is also found observationally, since Allen et al. (2001) report $14 \mu\text{G}$.

A.4. Cygnus A cluster

We use the electron density, temperature, and cool core radius reported in Mohr et al. (1999). We measure the RM dispersion to be 1200 m^{-2} from the map published by Dreher et al. (1987) after removing pixels from the map with extraordinary large RM jumps, which we associate with observational artefacts ($n\pi$ -ambiguities). Similar to the case of Hydra A, we see an asymmetry in the RM dispersion between the two lobes, which is a consequence of the different depth of the lobes (the Laing-Garrington effect: Laing 1988; Garrington et al. 1988). Unfortunately, the two radio lobes are located well beyond the cool core radius, which is even more true for their polarised regions used for RM measurements. Since we expect a declining magnetic-field strength as a function of radius, the reported RM dispersion is likely smaller than the one, which would be measured from a radio source located in the centre of the cool core, as discussed in Sect. 3.7 and illustrated in Fig. 2. The predicted central RM dispersion is a factor of two smaller than the peripherally measured one. With our current understanding of the geometry, it is fair to say that there is no apparent conflict between these numbers.

A.5. Perseus cluster

We take the central electron density, temperature, and the cool core radius from Churazov et al. (2003) and the cluster X-ray luminosity from David et al. (1993).

The Perseus cluster cool core exhibits diffuse radio emission, a radio mini-halo. One can apply the classical minimum-energy arguments to the radio halo data to search for the minimum of the sum of the magnetic and relativistic particle energy densities necessary to reproduce the radio synchrotron emission, and assume a constant proton to electron ratio k_p . Pfrommer & Enßlin (2004b) report a classical minimum field strength of $7.2_{-0.4}^{+4.5} \mu\text{G}$ (assuming $k_p = 1$), where the *confidence interval* is given by the requirement that the energy density should be within one *e*-fold from the minimum. Pfrommer & Enßlin (2004b) also develop and apply the hadronic minimum-energy criteria to the Perseus mini-halo. This criterion assumes that the relativistic electrons are injected by hadronic interactions of a relativistic proton population, which usually dominates the relativistic energy budget. No proton-to-electron factor k_p has to be assumed in this case, since the physics of the hadronic interaction determines this ratio. Applied to the Perseus radio halo, a very similar central field strength of $8.8_{-5.4}^{+13.8} \mu\text{G}$ was found. Our cool core model predicts a field strength of $7 - 13 \mu\text{G}$, which is well in agree-

ment with these findings. A significant lower central field value of about $1 - 3 \mu\text{G}$ was reported by Sanders et al. (2005), based on an Inverse Compton interpretation of a hard photon component in the X-ray spectra of the cool core region. Note, that if the hard photons flux would be due to another physical mechanism, the derived value will become a lower limit. If the Inverse Compton nature of the flux could be verified, this will be a very good field estimate in case of a non-intermittent field distribution. If there is significant magnetic intermittency, spatially inhomogeneous electron cooling can produce an anti-correlation between fields and relativistic electrons, which can easily lead to Inverse Compton based magnetic field estimates lower by a factor of two (Enßlin et al. 1999; Enßlin 2004).

As stated before, Fabian et al. (2003b) argued for a large-scale viscosity in the Perseus cluster cool core of at least $4 \cdot 10^{27} \text{ cm}^2/\text{s}$, which is in good agreement with the $1.6 \cdot 10^{28} \text{ cm}^2/\text{s}$ predicted in our $1 - d$ scenario.

A.6. Abell 2597

This cool core galaxy cluster has been observed with Chandra by McNamara et al. (2001). This observation has been reanalysed recently by Pollack et al. (2005). The gas parameters are taken from this reanalysis. The total luminosity used is taken from David et al. (1993).

Pollack et al. (2005) study also the polarisation properties of the central radio source in this cluster. They determine a RM dispersion of 1080 rad m^{-2} comparable to our expectations. They conclude that the cluster magnetic field has a minimum magnetic field strength of $2.1 \mu\text{G}$. Our model predicts a higher magnetic field strength of $7-12 \mu\text{G}$ which is in agreement with the lower limit of Pollack et al. (2005).

A.7. 3C31

The cool X-ray environment of the extended radio source 3C31 is associated with a group of galaxies. X-ray measurements suggest that this group shows properties similar to a cool core of a galaxy cluster. Therefore, it seems to be a good case to test our model in a different situation. The parameters for the gas were taken from Hardcastle et al. (2002). However we use the total luminosity from Komossa & Böhringer (1999).

Detailed RM measurements have been carried out by Laing et al. (in prep.). They determine the RM dispersion to be 25 rad m^{-2} (Laing, private communication).

A.8. Abell 85

We use the electron density, temperature, cool core radius, and luminosity reported in Mohr et al. (1999), and David et al. (1993). To our knowledge, no RM measurements or magnetic field estimates are available for the centre of this and all following clusters. Thus, our RM results are predictions.

A.9. Abell 2199

The parameters of the electron density profile as reported in Mohr et al. (1999) were used. The temperature of the cool core are taken from Voigt et al. (2002) and the total luminosity from David et al. (1993).

A.10. Virgo cluster

The Virgo cluster was observed with XMM-Newton by Matsushita et al. (2002). The gas parameters are taken from their analysis. However the total luminosity of David et al. (1993) is used for our calculations. The large difference between the cool core luminosity and the luminosity within the (larger) cooling radius is due to the extremely shallow density profile ($\beta \approx 0.5$) of Virgo. However, this should not affect our RM estimates too much, since only a $\beta \approx 0.25$ should lead to problems, as was argued in Sect. 3.7.

References

Allen, S. W. 1995, MNRAS, 276, 947

Allen, S. W., Schmidt, R. W., Fabian, A. C., & Ebeling, H. 2003, MNRAS, 342, 287

Allen, S. W., Taylor, G. B., Nulsen, P. E. J., et al. 2001, MNRAS, 324, 842

Böhringer, H., Matsushita, K., Churazov, E., Ikebe, Y., & Chen, Y. 2002, A&A, 382, 804

Batchelor, G. 1950, Proc. R. Soc. London A, 201, 405

Bertone, S., Vogt, C., & Enßlin, T. A. 2005, MNRAS submitted

Bicknell, G. V., Cameron, R. A., & Gingold, R. A. 1990, ApJ, 357, 373

Brüggen, M. & Kaiser, C. R. 2001, MNRAS, 325, 676

Brüggen, M., Kaiser, C. R., Churazov, E., & Enßlin, T. A. 2002, MNRAS, 331, 545

Brandenburg, A. & Subramanian, K. 2004, ArXiv Astrophysics e-prints

Brüggen, M., Hoeft, M., & Ruszkowski, M. 2005a, ArXiv Astrophysics e-prints

Brüggen, M., Ruszkowski, M., & Hallman, E. 2005b, ApJ, 630, 740

Carilli, C. L. & Taylor, G. B. 2002, Ann. Rev. of Astr. & Astrophys., 40, 319

Cen, R. 2005, ApJ, 620, 191

Chakrabarti, S. K., Rosner, R., & Vainshtein, S. I. 1994, Nature, 368, 434

Chandran, B. D. G. 2004, ApJ, 616, 169

Chandran, B. D. G. & Maron, J. L. 2004, ApJ, 602, 170

Cho, J., Lazarian, A., Honein, A., et al. 2003, ApJL, 589, L77

Cho, J. & Vishniac, E. T. 2000, ApJ, 538, 217

Churazov, E., Brüggen, M., Kaiser, C. R., Böhringer, H., & Forman, W. 2001, ApJ, 554, 261

Churazov, E., Forman, W., Jones, C., & Böhringer, H. 2003, ApJ, 590, 225

Churazov, E., Forman, W., Jones, C., Sunyaev, R., & Böhringer, H. 2004, MNRAS, 347, 29

Churazov, E., Sunyaev, R., Forman, W., & Böhringer, H. 2002, MNRAS, 332, 729

Clarke, T. E. 2004, Journal of Korean Astronomical Society, 37, 337

Clarke, T. E. & Enßlin, T. A. 2005, AJ submitted

Clarke, T. E., Kronberg, P. P., & Böhringer, H. 2001, ApJL, 547, L111

Crawford, C. S., Allen, S. W., Ebeling, H., Edge, A. C., & Fabian, A. C. 1999, MNRAS, 306, 857

Crawford, C. S., Hatch, N. A., Fabian, A. C., & Sanders, J. S. 2005, MNRAS, 363, 216

Daly, R. A. & Loeb, A. 1990, ApJ, 364, 451

David, L. P., Slyz, A., Jones, C., et al. 1993, ApJ, 412, 479

De Young, D. S. 1992, ApJ, 386, 464

Dennis, T. J. & Chandran, B. D. G. 2005, ApJ, 622, 205

Dolag, K., Bartelmann, M., & Lesch, H. 1999, A&A, 348, 351

Dolag, K., Bartelmann, M., & Lesch, H. 2002, A&A, 387, 383

Dolag, K., Jubelgas, M., Springel, V., Borgani, S., & Rasia, E. 2004, ApJL, 606, L97

Dolag, K., Schindler, S., Govoni, F., & Feretti, L. 2001, A&A, 378, 777

Dolag, K., Vogt, C., & Enßlin, T. A. 2005, MNRAS, 358, 726

Donahue, M., Mack, J., Voit, G. M., et al. 2000, ApJ, 545, 670

Dreher, J. W., Carilli, C. L., & Perley, R. A. 1987, ApJ, 316, 611

Edge, A. C. 2001, MNRAS, 328, 762

Edge, A. C. & Frayer, D. T. 2003, ApJL, 594, L13

Eilek, J. A. & Owen, F. N. 2002, ApJ, 567, 202

Enßlin, T. 2004, Journal of Korean Astronomical Society, 37, 439

Enßlin, T. A., Biermann, P. L., Klein, U., & Kohle, S. 1998a, A&A, 332, 395

Enßlin, T. A., Biermann, P. L., Kronberg, P. P., & Wu, X.-P. 1997, ApJ, 477, 560

Enßlin, T. A. & Heinz, S. 2002, A&A, 384, L27

Enßlin, T. A., Lieu, R., & Biermann, P. L. 1999, A&A, 344, 409

Enßlin, T. A. & Vogt, C. 2003, A&A, 401, 835

Enßlin, T. A., Vogt, C., Clarke, T. E., & Taylor, G. B. 2003, ApJ, 597, 870

Enßlin, T. A., Wang, Y., Nath, B. B., & Biermann, P. L. 1998b, A&A, 333, L47

Fabian, A. C., Nulsen, P. E. J., & Canizares, C. R. 1991, A&A Rev., 2, 191

Fabian, A. C., Sanders, J. S., Allen, S. W., et al. 2003a, MNRAS, 344, L43

Fabian, A. C., Sanders, J. S., Crawford, C. S., et al. 2003b, MNRAS, 344, L48

Feretti, L., Dallacasa, D., Giovannini, G., & Tagliani, A. 1995, A&A, 302, 680

Feretti, L., Dallacasa, D., Govoni, F., et al. 1999, A&A, 344, 472

Fujita, Y., Suzuki, T. K., & Wada, K. 2004, ApJ, 600, 650

Garrington, S. T., Leahy, J. P., Conway, R. G., & Laing, R. A. 1988, Nature, 331, 147

Ge, J. P. & Owen, F. N. 1993, AJ, 105, 778

Goldman, I. & Rephaeli, Y. 1991, ApJ, 380, 344

Goldreich, P. & Sridhar, S. 1997, ApJ, 485, 680

Goldshmidt, O. & Rephaeli, Y. 1993, ApJ, 411, 518

Govoni, F. & Feretti, L. 2004, International Journal of Modern

Physics D, 13, 1549

Govoni, F., Taylor, G. B., Dallacasa, D., Feretti, L., & Giovannini, G. 2001, *A&A*, 379, 807

Hansen, L., Jorgensen, H. E., & Norgaard-Nielsen, H. U. 1995, *A&A*, 297, 13

Hardcastle, M. J., Worrall, D. M., Birkinshaw, M., Laing, R. A., & Bridle, A. H. 2002, *MNRAS*, 334, 182

Haugen, N. E., Brandenburg, A., & Dobler, W. 2004, *Phys. Rev. E*, 70, 016308

Heckman, T. M., Baum, S. A., van Breugel, W. J. M., & McCarthy, P. 1989, *ApJ*, 338, 48

Heinz, S., Reynolds, C. S., & Begelman, M. C. 1998, *ApJ*, 501, 126

Hoeft, M. & Brüggen, M. 2004, *ApJ*, 617, 896

Ikebe, Y., Makishima, K., Ezawa, H., et al. 1997, *ApJ*, 481, 660

Inogamov, N. A. & Sunyaev, R. A. 2003, *Astronomy Letters*, 29, 791

Jaffe, W. 1980, *ApJ*, 241, 925

Jaffe, W. & Bremer, M. N. 1997, *MNRAS*, 284, L1

Johnston-Hollitt, M. & Ekers, R. D. 2004, *ArXiv:astro-ph/0411045*

Jubelgas, M., Springel, V., & Dolag, K. 2004, *MNRAS*, 351, 423

Kaiser, C. R., Pavlovski, G., Pope, E. C. D., & Fangohr, H. 2005, *MNRAS*, 359, 493

Kazantsev, A. 1967, *J. Exp. Theor. Phys.*, 53, 1806

Kim, K.-T., Kronberg, P. P., & Tribble, P. C. 1991, *ApJ*, 379, 80

Komossa, S. & Böhringer, H. 1999, *A&A*, 344, 755

Kronberg, P. P., Dufton, Q. W., Li, H., & Colgate, S. A. 2001, *ApJ*, 560, 178

Kronberg, P. P., Lesch, H., & Hopp, U. 1999, *ApJ*, 511, 56

Laing, R. A. 1988, *Nature*, 331, 149

Loewenstein, M. & Fabian, A. C. 1990, *MNRAS*, 242, 120

Longcope, D. W., McLeish, T. C. B., & Fisher, G. H. 2003, *ApJ*, 599, 661

Malyshkin, L. 2001, *ApJ*, 554, 561

Matsushita, K., Belsole, E., Finoguenov, A., & Böhringer, H. 2002, *A&A*, 386, 77

Mazzotta, P., Brunetti, G., Giacintucci, S., Venturi, T., & Bardelli, S. 2004, *Journal of Korean Astronomical Society*, 37, 381

McNamara, B. R., Wise, M. W., Nulsen, P. E. J., et al. 2001, *ApJL*, 562, L149

Mohr, J. J. & Evrard, A. E. 1997, *ApJ*, 491, 38

Mohr, J. J., Mathiesen, B., & Evrard, A. E. 1999, *ApJ*, 517, 627

Narayan, R. & Medvedev, M. V. 2001, *ApJL*, 562, L129

Nipoti, C. & Binney, J. 2004, *MNRAS*, 349, 1509

O'Dea, C. P., Payne, H. E., & Kocevski, D. 1998, *AJ*, 116, 623

Oegerle, W. R., Cowie, L., Davidsen, A., et al. 2001, *ApJ*, 560, 187

Peres, C. B., Fabian, A. C., Edge, A. C., et al. 1998, *MNRAS*, 298, 416

Perley, R. A. & Taylor, G. B. 1991, *AJ*, 101, 1623

Pfrommer, C. & Enßlin, T. A. 2004a, *A&A*, 413, 17

Pfrommer, C. & Enßlin, T. A. 2004b, *MNRAS*, 352, 76

Pollack, L. K., Taylor, G. B., & Allen, S. W. 2005, *MNRAS*, 359, 1229

Pringle, J. E. 1989, *MNRAS*, 239, 479

Quilis, V., Bower, R. G., & Balogh, M. L. 2001, *MNRAS*, 328, 1091

Rees, M. J. 1987, *QJRAS*, 28, 197

Reynolds, C. S., Heinz, S., & Begelman, M. C. 2002, *MNRAS*, 332, 271

Reynolds, C. S., McKernan, B., Fabian, A. C., Stone, J. M., & Vernaleo, J. C. 2005, *MNRAS*, 357, 242

Roettiger, K., Burns, J. O., & Stone, J. M. 1999a, *ApJ*, 518, 603

Roettiger, K., Stone, J. M., & Burns, J. O. 1999b, *ApJ*, 518, 594

Roland, J. 1981, *A&A*, 93, 407

Rudnick, L. & Blundell, K. M. 2003, *ApJ*, 588, 143

Ruszkowski, M. & Begelman, M. C. 2002, *ApJ*, 581, 223

Ruszkowski, M., Brüggen, M., & Begelman, M. C. 2004, *ApJ*, 615, 675

Ruzmaikin, A., Sokolov, D., & Shukurov, A. 1989, *MNRAS*, 241, 1

Salomé, P. & Combes, F. 2003, *A&A*, 412, 657

Sanders, J. S. & Fabian, A. C. 2002, *MNRAS*, 331, 273

Sanders, J. S., Fabian, A. C., & Dunn, R. J. H. 2005, *MNRAS*, 360, 133

Schekochihin, A., Cowley, S., Maron, J., & Malyshkin, L. 2002, *Phys. Rev. E*, 65, 016305

Schekochihin, A. A. & Cowley, S. C. 2006, *ArXiv Astrophysics e-prints*

Schekochihin, A. A., Cowley, S. C., Kulsrud, R. M., Hammett, G. W., & Sharma, P. 2005, *ApJ*, 629, 139

Schuecker, P., Finoguenov, A., Miniati, F., Böhringer, H., & Briel, U. G. 2004, *A&A*, 426, 387

Smith, E. P., Bohlin, R. C., Bothun, G. D., et al. 1997, *ApJ*, 478, 516

Soker, N. 2003, *MNRAS*, 342, 463

Soker, N. 2004, *MNRAS*, 350, 1015

Soker, N., Blanton, E. L., & Sarazin, C. L. 2004, *A&A*, 422, 445

Soker, N. & Pizzolato, F. 2005, *ApJ*, 622, 847

Soker, N. & Sarazin, C. L. 1990, *ApJ*, 348, 73

Sokolov, D. D., Ruzmaikin, A. A., & Shukurov, A. 1990, in *IAU Symp. 140: Galactic and Intergalactic Magnetic Fields*, 499–502

Subramanian, K. 1999, *Physical Review Letters*, 83, 2957

Subramanian, K., Shukurov, A., & Haugen, N. E. L. 2006, *MNRAS*, 99

Sunyaev, R. A., Norman, M. L., & Bryan, G. L. 2003, *Astronomy Letters*, 29, 783

Taylor, G. B., Fabian, A. C., & Allen, S. W. 2002, *MNRAS*, 334, 769

Taylor, G. B., Govoni, F., Allen, S. W., & Fabian, A. C. 2001, *MNRAS*, 326, 2

Taylor, G. B. & Perley, R. A. 1993, *ApJ*, 416, 554

Tribble, P. C. 1993, *MNRAS*, 263, 31

Vogt, C., Dolag, K., & Enßlin, T. A. 2005, *MNRAS*, 358, 732

Vogt, C. & Enßlin, T. A. 2003, *A&A*, 412, 373

Vogt, C. & Enßlin, T. A. 2005, *A&A*, 434, 67

Voigt, L. M. & Fabian, A. C. 2004, *MNRAS*, 347, 1130

Voigt, L. M., Schmidt, R. W., Fabian, A. C., Allen, S. W., &

Johnstone, R. M. 2002, MNRAS, 335, L7
Völk, H. J. & Atoyan, A. M. 2000, ApJ, 541, 88
White, D. A. 2000, MNRAS, 312, 663
Widrow, L. M. 2002, Reviews of Modern Physics, 74, 775
Zeldovich, Y. B., Ruzmaikin, A. A., & Sokoloff, D. D. 1990,
The almighty chance (World Scientific Lecture Notes in
Physics, Singapore: World Scientific Publication, 1990)